

Unified First-Principles Formula for Time-Resolved ARPES Spectra of Coherent and Incoherent Excitons

Gianluca Stefanucci^{1,2} and Enrico Perfetto^{1,2}

¹*Dipartimento di Fisica, Università di Roma Tor Vergata, Via della Ricerca Scientifica 1, 00133 Rome, Italy*

²*INFN, Sezione di Roma Tor Vergata, Via della Ricerca Scientifica 1, 00133 Rome, Italy*

Despite major experimental progresses in time-resolved and angle-resolved photoemission spectroscopy, a quantitative, microscopic framework for interpreting exciton-induced modifications of electronic band structures – applicable even beyond the low-density limit – is still lacking. Here we close this gap by introducing a unified approach that links the dynamics of coherent and incoherent excitons to distinct and experimentally observable excitonic sidebands. Our central result is a general, first-principles formula for time-resolved photoemission spectra, applicable across a broad range of temperatures, excitation densities, and pump–probe delays. This advance provides a predictive tool for quantitatively tracking excitonic dynamics in complex materials.

Introduction.— The concept of excitons as quasiparticles in semiconductors and insulators has long been central to the interpretation of optical spectra, where it underpins the understanding of subgap resonances and above-gap structures in absorbance and reflectance measurements [1]. Optical probes, however, are fundamentally restricted to bright, zero-center-of-mass-momentum excitons and primarily access their energies. By contrast, angle-resolved photoemission spectroscopy (ARPES) reveals a far richer and more detailed picture [2–4]. In particular, time-resolved ARPES (TR-ARPES) has recently emerged as a powerful platform for exciton physics, enabling direct access to bright, momentum-dark, and spin-dark excitons [5–12]. Beyond exciton energies, TR-ARPES uniquely resolves excitonic wavefunctions in both band and momentum space [13–16].

Although TR-ARPES [17] has led to informative experimental spectra, a rigorous connection with the underlying exciton dynamics is still lacking. After pumping below the bandgap, the nonequilibrium exciton fluid [18–22] drives the motion of the nuclear lattice. The scattering between electrons and phonons destroys exciton coherence [23–28] and diffuses excitons [29–32]. Bright coherent excitons are converted – typically in less than a few hundreds of femtoseconds [33–35] – into bright and dark incoherent excitons. TR-ARPES spectra of *coherent* excitons have been successfully described [36–40]. However, a first principles many-body framework for the *incoherent* regime – applicable even beyond the domain of low excitation densities – remains underdeveloped [41–44]. In this Letter, we identify distinct signatures of coherent and incoherent excitons in the TR-ARPES signal and provide a unified theory of excitonic sidebands emerging from different exciton states. The main finding is a ready-to-use first-principles formula for interpreting TR-ARPES spectra across a wide range of temperatures, excitation densities and pump–probe delays.

Photocurrent.— The rate of photoelectrons with energy ϵ and parallel momentum \mathbf{k} , ejected by a high-energy probe pulse $a(t) = ae^{-i\omega_0 t} + \text{h.c.}$ impinging on the crystal after a delay τ from the pump, is proportional to [41, 45]

$$I_{\mathbf{k}}(\tau, \epsilon) \propto -i|a|^2 \sum_{\mu\mu'} D_{\mu\mathbf{k}}(\epsilon) D_{\mu'\mathbf{k}}^*(\epsilon) G_{\mu\mu'\mathbf{k}}^<(\tau, \omega_0 - \epsilon), \quad (1)$$

where $D_{\mu\mathbf{k}}(\epsilon)$ is the photoemission matrix element for an elec-

tron with band-momentum index $(\mu\mathbf{k})$. Henceforth, we use $\mu = c$ for conduction bands and $\mu = v$ for valence bands. The nonequilibrium electronic properties of the crystal are encoded in the Fourier transform, $G^<(\tau, \omega)$, of the lesser Green's function $G^<(t, t')$ with respect to the time-difference $t - t'$ for a given center-of-mass-time (delay) $\tau = (t + t')/2$. In the quasiparticle approximation $G_{\mu\mu'\mathbf{k}}^<(\tau, \omega) = \delta_{\mu\mu'} 2\pi i f_{\mu\mathbf{k}}(\tau) \delta(\omega - \epsilon_{\mu\mathbf{k}}(\tau))$, and the spectrum is peaked at the quasiparticle energies $\epsilon_{\mu\mathbf{k}}(\tau)$ – with an intensity proportional to the nonequilibrium populations $f_{\mu\mathbf{k}}(\tau)$. Since our primary interest is in the excitonic sidebands appearing above the valence band maximum, we focus exclusively on the contribution of conduction electrons to the photoemission signal. Consequently, we restrict the sum over μ, μ' in Eq. (1) to the conduction bands.

TR-ARPES formula.— The interacting nonequilibrium $G^<$ for conduction electrons can be calculated from [46]

$$G_{\mathbf{k}}^<(\tau, \omega) = G_{\mathbf{k}}^R(\tau, \omega) \Sigma_{\mathbf{k}}^<(\tau, \omega) G_{\mathbf{k}}^A(\tau, \omega), \quad (2)$$

where all quantities are matrices with conduction band indices. We remark that this way of calculating $G^<$ differs from earlier attempts [41, 42], which rely on the fluctuation-dissipation *ansatz* $G_{\mathbf{k}}^<(\tau, \omega) = i f(\omega - \mu_c) A_{\mathbf{k}}(\tau, \omega)$, where f is the Fermi function with a conduction-band chemical potential μ_c fixed by the excitation density, and $A_{\mathbf{k}}(\tau, \omega)$ is the nonequilibrium spectral function. This *ansatz* is problematic for frequencies ω below the gap since, at finite temperature and/or out of equilibrium, the addition and removal energies overlap. The retarded and advanced Green's functions

$$G_{\mathbf{k}}^R(\tau, \omega) = [G_{\mathbf{k}}^A(\tau, \omega)]^\dagger = [\omega - \mathcal{E}_{\mathbf{k}}(\tau) - \Sigma_{\mathbf{k}}^R(\tau, \omega)], \quad (3)$$

with $[\mathcal{E}_{\mathbf{k}}(\tau)]_{\mu\mu'} \equiv \delta_{\mu\mu'} \epsilon_{\mu\mathbf{k}}(\tau)$, and the lesser Green's function in Eq. (2) can be calculated once an approximation for the electronic self-energy Σ is available.

Let us consider pump fields with frequencies below the bandgap, ensuring that only discrete states are explored during the time evolution. We demonstrate below that Hartree plus statically screened exchange (HSEX) effectively capture the coherent regime, while T-matrix plus exchange accurately describes the incoherent regime. Remarkably, the full self-

energy can be compactly expressed as

$$\Sigma_{cc'k}^R(\tau, \omega) = \sum_{\lambda Qv} \sigma_{cc'k}^{\lambda Qv}(\tau, \omega), \quad (4a)$$

$$\begin{aligned} \Sigma_{cc'k}^<(\tau, \omega) = & \sum_{\lambda Qv} f(\omega - E_{\lambda Q}(\tau) - \epsilon_{v k - Q}(\tau)) \\ & \times [\sigma_{cc'k}^{\lambda Qv}(\tau, \omega) - \sigma_{cc'k}^{\lambda Qv*}(\tau, \omega)], \end{aligned} \quad (4b)$$

where the sum runs over all valence bands and over all exciton states λ of momentum Q . In the Fermi function of Eq. (4b), the quasiparticle energies $\epsilon_{\mu k}(\tau)$ and exciton energies $E_{\lambda Q}(\tau)$ are those of the *nonequilibrium* system. The key quantity in Eq. (4) is the function

$$\sigma_{cc'k}^{\lambda Qv}(\tau, \omega) = K_{cvk}^{\lambda Q} \frac{N_{\lambda Q}(\tau)}{\omega - E_{\lambda Q}(\tau) - \epsilon_{v k - Q}(\tau) + i\eta} K_{c'vk}^{\lambda Q*} - i\eta, \quad (5)$$

where η is a positive infinitesimal, and the amplitude

$$K_{cvk}^{\lambda Q} = (\epsilon_{ck}^{\text{eq}} - \epsilon_{v k - Q}^{\text{eq}} - E_{\lambda Q}^{\text{eq}}) A_{cvk - Q}^{\lambda Q} \quad (6)$$

is expressed in terms of the equilibrium band structure $\epsilon_{\mu k}^{\text{eq}}$, exciton energies $E_{\lambda Q}^{\text{eq}}$ and wavefunctions $A_{cvk}^{\lambda Q}$. Notably, the full self-energy depends only on the *total* number of excitons at the probing time τ [32]

$$N_{\lambda Q}(\tau) = \delta_{Q,0} |\rho_{\lambda}(\tau)|^2 + N_{\lambda Q}^{\text{inc}}(\tau), \quad (7)$$

with $|\rho_{\lambda}|^2$ the number of coherent excitons, and $N_{\lambda Q}^{\text{inc}}$ the number of incoherent excitons. In Appendix A we present a practical method to extract the nonequilibrium energies $\epsilon_{\mu k}(\tau)$ and $E_{\lambda Q}(\tau)$ directly from $N_{\lambda Q}(\tau)$. Equations (2-5) are the main result of this Letter. They provide a first-principles formula to calculate TR-ARPES spectra for any pump-probe delay, and for a wide range of temperatures and excitation densities. The only input quantities are the exciton populations $N_{\lambda Q}(\tau)$, which can be determined by, e.g., solving the excitonic Bloch equations [32, 34, 47, 48].

Coherent regime.— Here we briefly revisit the theory of the coherent regime, and offer an alternative perspective. Without any loss of generality we set the time origin, $t = 0$, after the action of the pump pulse. For weak pumping the excitation density is low, and the state of the system at positive times is given by the quantum superposition $|\Psi(t)\rangle = |\Psi_g\rangle + \sum_{\lambda} \rho_{\lambda}(t) |\lambda 0\rangle$, where $|\Psi_g\rangle$ is the ground state and $|\lambda Q\rangle = \sum_{cvk} A_{cvk}^{\lambda Q} \hat{d}_{ck+Q}^{\dagger} \hat{d}_{vk} |\Psi_g\rangle$ are the exciton states of momentum Q – here $\hat{d}_{\mu k}$ is the annihilation operator for electrons in band μ with momentum k . As the pump pulse can only excite bright excitons, $|\Psi(t)\rangle$ contains exclusively excitons of vanishing momentum, $Q = 0$. The coefficients $\rho_{\lambda}(t) = \sum_{cvk} A_{cvk}^{\lambda Q*} \langle \Psi(t) | \hat{d}_{vk}^{\dagger} \hat{d}_{ck} | \Psi(t) \rangle$ are the exciton polarizations, and their square modulus yield the number of coherent excitons, see Eq. (7). The system is described by the state $|\Psi(t)\rangle$ up to times smaller than the exciton lifetimes. Such time window defines the coherent regime. From the knowledge of $|\Psi(t)\rangle$ we can directly calculate $G^<$, see Appendix B,

and hence the TR-ARPES spectrum. We refer to this strategy as the *Lehmann approach*, since it is based on expanding the many-body state in eigenstates of the Hamiltonian. The same $G^<$ can be obtained from Eq. (2) using the HSEX self-energy, see Eq. (12). The explicit form of the HSEX self-energy can be readily derived by projecting the equations of motion for the Green's function [36, 37] onto the conduction-band subspace. The final result is Eqs. (4) with σ evaluated in $N_{\lambda Q} = \delta_{Q,0} |\rho_{\lambda}|^2$, see Appendices C and D for details. The advantage of the many-body formulation over the Lehmann approach is that it successfully extends beyond the domain of low excitation densities [40].

Incoherent regime.— In the incoherent regime the polarization ρ_{λ} vanishes, and consequently the HSEX self-energy in Eqs. (4) vanishes too. In this regime, the electronic subsystem is described by an ensemble of bright and dark incoherent excitons. The transition from a pure state to an ensemble is a general phenomenon in systems interacting with a bath, such as electrons interacting with phonons in our case. It has been demonstrated in an exactly solvable two-band model [27, 49], and it is also a consequence of the excitonic Bloch equations [32, 34, 47, 48].

A heuristic theory for the photocurrent in the incoherent regime can be effectively developed for low excitation densities. According to the excitonic Bloch equations the incoherent ensemble is described by the many-body density matrix $\hat{\rho} = |\Psi_g\rangle\langle\Psi_g| + \sum_{\lambda Q} N_{\lambda Q}^{\text{inc}} |\lambda Q\rangle\langle\lambda Q|$. From the knowledge of $\hat{\rho}$ we can calculate $G^<$, see Appendix B, which in turn allows us to determine the TR-ARPES spectrum. This is the Lehmann approach of the incoherent regime [26, 27, 41, 43, 50]. Establishing the many-body diagrammatic approximation underlying this approach would lift the low-density constraint, and pave the way toward a fully first-principles treatment of TR-ARPES spectra in the incoherent regime.

At present, the state-of-the-art many-body approximation is largely based on the T-matrix diagrams [41, 42, 51, 52]. Previous studies reported excitonic sidebands appearing as replicas of the conduction bands [41, 42], in apparent contradiction to the Lehmann approach, which instead predicts replicas of the valence bands. Another issue pertains to the intensity of the photoemission signal, proportional to $|A_{cvk}^{\lambda Q}|^2$. The exciton wavefunctions satisfy the Bethe Salpeter equation (BSE), whose kernel is the sum of the bare Coulomb interaction v (direct term) and the screened interaction W (exchange term) [1, 46, 53], i.e.,

$$(\epsilon_{ck+Q}^{\text{eq}} - \epsilon_{vk}^{\text{eq}}) A_{cvk}^{\lambda Q} - \sum_{c'v'k'} K_{cvk, c'v'k'}^Q A_{c'v'k'}^{\lambda Q} = E_{\lambda Q}^{\text{eq}} A_{cvk}^{\lambda Q}, \quad (8)$$

with

$$K_{cvk, c'v'k'}^Q = W_{ck+Q v'k' v k c'k' + Q} - v_{ck+Q v'k' c'k' + Q v k}. \quad (9)$$

Thus, a pure T-matrix self-energy (containing only W) cannot yield the Lehmann intensity of the signal.

To reconcile many-body theory with the Lehmann approach we consider the four self-energy diagrams of Fig. 1 – the gray circle is the exchange-correlation (xc) function L , the wiggly

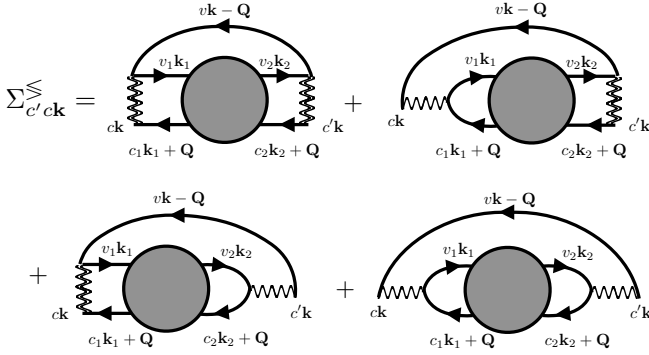


FIG. 1. TX self-energy for the Green's function in the incoherent regime. We represent Green's functions G with solid lines, bare interactions v with wiggly lines, screened interactions W with wiggly lines and the xc function L with a gray circle.

line is the bare interaction v , and the double wiggly line is the statically screened interaction W . The first diagram in Fig. 1 is the T-matrix self-energy, and we refer to the sum of all four diagrams as the T-matrix plus exchange (TX) self-energy. Notice that the zeroth order xc function is simply GG . Consequently, the lowest-order T-matrix diagram has the same topology as the (second-Born) bubble diagram, except that *both* interaction lines are screened. This raises the issue of a possible double counting of screening diagrams, which we address below.

The diagrammatic equation of Fig. 1 is an approximation for the *lesser* and *greater* self-energy, not for the time (or contour) ordered Σ . Accordingly, the bubble diagram with two W lines does not emerge from T-matrix, rather from GW. Indeed, $\Sigma_{GW}^< = iG^<W^< = iG^<W^R P^< W^A$ where $P^< = iG^<G^>$ [46]. Evaluating the screened interaction in the static approximation, $W^R = W^A = W$, we recover the lowest order (first) diagram in Fig. 1. Thus, there is no double counting issue. We also observe that the first diagram does not include the *full* GW self-energy, since the bottom Green's function is summed over conduction bands only. The missing contributions are recovered by adding the fourth diagram in Fig. 1. In fact, this diagram has the structure $Gv\chi v = G(W - v)$, χ being the density response function, and G is summed over the valence bands. In summary, the lesser and greater self-energies of Fig. 1 incorporate the full GW self-energy, but handle W differently depending on the Green's function band indices. If G has conduction indices then W is statically screened, whereas for valence indices W is dynamically screened.

Taking into account the definition of the HSEX kernel in Eq. (9), the TX self-energy of Fig. 1 can be written as

$$\begin{aligned} \Sigma_{cc'k}^{\leq\leq}(t, t') = & -i^2 \sum_{\substack{c_1 c_2 v_1 v_2 v \\ k_1 k_2 Q}} K_{cvk-Q, c_1 v_1 k_1}^Q L_{c_1 v_1 k_1, c_2 v_2 k_2}^{Q\leq\leq}(t, t') \\ & \times K_{c'v'k-Q, c_2 v_2 k_2}^{Q*} G_{v'k-Q}^{\leq\leq}(t, t'), \end{aligned} \quad (10)$$

from which we can extract the retarded self-energy according

to

$$\Sigma_{cc'k}^R(\tau, \omega) = i \int \frac{d\omega'}{2\pi} \frac{\Sigma_{cc'k}^<(\tau, \omega) - \Sigma_{cc'k}^<(\tau, \omega')}{\omega - \omega' + i\eta} - i\eta. \quad (11)$$

Expanding the xc function L in the excitonic basis [32, 41], and approximating the Green's function at the quasiparticle level, we obtain Eq. (4a) with σ evaluated in $N_{\lambda Q} = N_{\lambda Q}^{\text{inc}}$ – we refer the reader to Appendix E for the derivation. This result agrees with that of a pure T-matrix calculation [42] only if the exciton energies and wavefunctions remain unchanged upon setting the bare v to zero in Eq. (9), which is generally not the case.

Equation (10) is only used to extract Σ^R . The lesser self-energy in Eq. (2) is derived from σ according to Eq. (4b), ensuring consistency with the self-energy in the coherent regime, see Appendix D. As we see below [Eq. (16)], such consistency is essential not only for recovering the results of the Lehmann approach but also for extending the theory beyond the low-density limit.

Low density.— In the low-density limit $N_{\lambda Q}$ is infinitesimal, and $E_{\lambda Q}(\tau)$ and $\epsilon_{\mu k}(\tau)$ are well approximated by their equilibrium values. To lowest order in the excitation density, Eq. (2) yields

$$\begin{aligned} G_{cc'k}^<(\tau, \omega) = & \lim_{\eta \rightarrow 0} \frac{1}{\omega - \epsilon_{ck}^{\text{eq}} + i\eta} \Sigma_{cc'k}^<(\tau, \omega) \frac{1}{\omega - \epsilon_{c'k}^{\text{eq}} - i\eta} \\ = & 2\pi i \sum_{\lambda Q v} N_{\lambda Q}(\tau) A_{cvk-Q}^{\lambda Q} A_{c'v'k-Q}^{\lambda Q*} \delta(\omega - E_{\lambda Q}^{\text{eq}} - \epsilon_{v'k-Q}^{\text{eq}}), \end{aligned} \quad (12)$$

where we use Eq. (6). This result agrees with the Lehmann approach both in the coherent ($N_{\lambda Q} = \delta_{Q0}|\rho_\lambda|^2$) and incoherent ($N_{\lambda Q} = N_{\lambda Q}^{\text{inc}}$) regimes, see Appendix B. It also agrees with the removal part of the spectral function in the incoherent regime presented in Ref. [42].

Inserting Eq. (12) in the photocurrent formula Eq. (1) we find

$$\begin{aligned} I_k(\tau, \epsilon) \propto & |a|^2 \sum_{\lambda Q} N_{\lambda Q}(\tau) \sum_v \left| \sum_c D_{ck}(\epsilon) A_{cvk-Q}^{\lambda Q} \right|^2 \\ & \times 2\pi \delta(\epsilon_{v'k-Q}^{\text{eq}} + E_{\lambda Q}^{\text{eq}} - \epsilon + \omega_0). \end{aligned} \quad (13)$$

This formula extends the theory of Refs. [41, 43] to multiple bands, and corrects the ansatz in Ref. [50] by placing the sum over conduction bands inside the square modulus. According to Eq. (13), a λQ exciton generates a replica of the valence bands shifted in energy by $E_{\lambda Q}^{\text{eq}}$ and in momentum by Q , see Fig. 2(c). It is worth observing that if the lowest-energy exciton, say λ_0 , is bright, and if we pump resonantly with it, then $\rho_\lambda(\tau) \propto \delta_{\lambda\lambda_0}$ (resonance condition). As phonons do not scatter the exciton into higher energy states, the coherent λ_0 -exciton can only transition into an incoherent λ_0 -exciton of vanishing momentum. Considering the conservation of the total number of excitons [32], we infer that $N_{\lambda Q}(\tau) \propto \delta_{\lambda\lambda_0}\delta_{Q0}$ is independent of τ . Thus, in this scenario, the TR-ARPES signal is identical in the coherent and incoherent regimes [54].

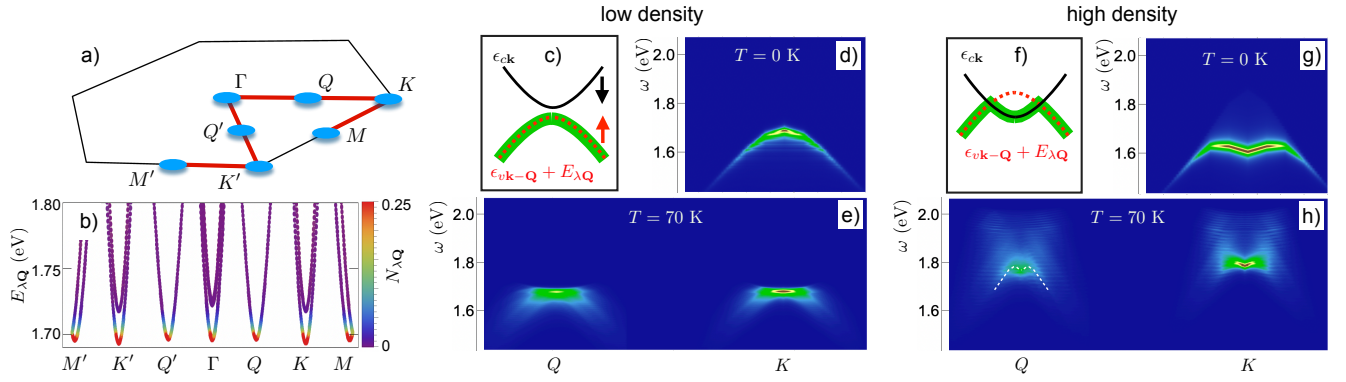


FIG. 2. (a) First Brillouin zone and location of a few high symmetry points. (b) Exciton band structure of the equilibrium WSe₂ ML along the red path illustrated in panel (a) – curves are colored according to the thermal occupation of excitons at temperature $T = 70$ K and excitation density $n_c = 10^{13} \text{ cm}^{-2}$. (c,f) Illustration of conduction band and replica of valence band at low [panel (c)] and moderate [panel (f)] excitation densities. (d,e,g,h) TR-ARPES spectrum (in arbitrary units) for low [panels (d,e)] and high [panels (g,h)] excitation densities at different temperatures: $n_c = 10^{11} \text{ cm}^{-2}$ and $T = 0$ K [panel (d)]; $n_c = 10^{11} \text{ cm}^{-2}$ and $T = 70$ K [panel (e)]; $n_c = 4 \times 10^{12} \text{ cm}^{-2}$ and $T = 0$ K [panel (g)]; $n_c = 10^{13} \text{ cm}^{-2}$ and $T = 70$ K [panel (h)].

Revealing the coherence of the system with TR-ARPES requires a probe field with a duration comparable to the exciton period [37].

An important feature of Eq. (12) is that the total number of carriers in the conduction band is given by

$$N_c(\tau) = -i \int \frac{d\omega}{2\pi} \sum_{ck} G_{cck}^<(\tau, \omega) = \sum_{\lambda Q} N_{\lambda Q}(\tau), \quad (14)$$

where the normalization of the exciton wavefunctions $\sum_{cvk} |A_{cvk}^{\lambda Q}|^2 = 1$ has been used. In other words, in the low density limit N_c is the same as the total number of excitons, as it should be. We remark that this property would not be satisfied if we had included only the T-matrix diagram in the self-energy.

Beyond low density.— The formula Eq. (2) for $G^<$ simplifies if the wavefunction of the occupied exciton states have a predominant contribution on a single conduction band and valence band, say c_0 and v_0 . In this case, $K_{cvk}^{\lambda Q} = \delta_{cc_0} \delta_{vv_0} K_{c_0 v_0 k}^{\lambda Q}$, and the quantity σ in Eq. (5) has one single nonvanishing entry for $c = c' = c_0$. This implies that also the self-energy is nonvanishing only for $c = c' = c_0$. Defining $\Delta_k^{\lambda Q}(\tau) \equiv \sqrt{N_{\lambda Q}(\tau)} K_{c_0 v_0 k}^{\lambda Q}$, and omitting the dependence of the various quantities on τ , we have

$$G_{c_0 c_0 k}^R(\omega) = \frac{1}{\omega - \epsilon_{c_0 k} - \sum_{\lambda Q} \frac{|\Delta_k^{\lambda Q}|^2}{\omega - E_{\lambda Q} - \epsilon_{v_0 k-Q} + i\eta} + i\eta}. \quad (15)$$

To gain insight into this problem, we assume that only a discrete number of excitons $\lambda_j Q_j$ are populated, and that $\Delta_k^j \equiv \Delta_k^{\lambda_j Q_j}$ are nonvanishing in small and nonoverlapping regions \mathcal{R}^j of the first Brillouin zone. Then, for $k \in \mathcal{R}^j$ only $\lambda_j Q_j$ contributes to the sum in the denominator of Eq. (15). This allows us to calculate $G_{c_0 c_0 k}^<$ analytically, see Appendix C for

details, and find

$$G_{c_0 c_0 k}^<(\omega) \simeq 2\pi i \sum_j \frac{E_{\lambda_j Q_j} + \epsilon_{v_0 k-Q_j} - E_{k,j}^-}{E_{k,j}^+ - E_{k,j}^-} \delta(\omega - E_{k,j}^-), \quad (16)$$

where

$$E_{k,j}^\pm = \frac{1}{2} \left[\epsilon_{c_0 k} + E_{\lambda_j Q_j} + \epsilon_{v_0 k-Q_j} \right. \\ \left. \pm \sqrt{(\epsilon_{c_0 k} - E_{\lambda_j Q_j} - \epsilon_{v_0 k-Q_j})^2 + 4|\Delta_k^j|^2} \right]. \quad (17)$$

To lowest order in $|\Delta_k^j|$ (low density limit) we can approximate the argument of the Dirac-delta as $E_{k,j}^- \simeq E_{\lambda_j Q_j}^{\text{eq}} + \epsilon_{v_0 k-Q_j}^{\text{eq}}$, and the prefactor of the Dirac-delta as $|\Delta_k^j|^2 / (\epsilon_{c_0 k}^{\text{eq}} - E_{\lambda_j Q_j}^{\text{eq}} - \epsilon_{v_0 k-Q_j}^{\text{eq}})^2 = N_{\lambda_j Q_j} |A_{c_0 v_0 k}^{\lambda_j Q_j}|^2$; the resulting $G^<$ correctly agrees with Eq. (12). Increasing the excitation density, the nonequilibrium energy $E_{\lambda_j Q_j}(\tau) + \epsilon_{v_0 k-Q_j}(\tau)$ might overcome $\epsilon_{c_0 k}(\tau)$, leading to a hybridization (proportional to $|\Delta_k^j|$) between the conduction band and the replica of the valence band, see Fig. 2(f). This scenario has been thoroughly investigated in the coherent regime [36, 37, 39] – hence for $\mathbf{Q} = \mathbf{0}$ – and is associated with a BEC-BCS crossover of the coherent exciton fluid [20, 21]. Our result in Eq. (16) indicates that the same phenomenon can also occur in the incoherent regime. In particular, the excitonic sidebands induced by a sizable population of incoherent excitons of momentum \mathbf{Q} might resemble the conduction bands hybridized with a \mathbf{Q} -shifted replica of the valence bands.

TR-ARPES in WSe₂ monolayer.— We consider a WSe₂ monolayer (ML) at low ($n_c \sim 10^{11} \text{ cm}^{-2}$) and moderate ($n_c \sim 10^{13} \text{ cm}^{-2}$) excitation densities $n_c = N_c/A$, where A is the area of the sample. The WSe₂ ML is a direct gap semiconductor, with a calculated bandgap at the K and K' points

[Fig. 2(a)] estimated to be ~ 2 eV [55]. For sufficiently long times after pumping, the exciton populations follow a Bose distribution $N_{\lambda Q} = [e^{(E_{\lambda Q} - \mu_X)/T} - 1]^{-1}$, where T is the temperature and μ_X is self-consistently calculated from Eq. (14). In Fig. 2(b) we show the equilibrium exciton band structure, and how excitons are distributed at temperature $T = 70$ K; numerical details are reported in Appendix F. The low-energy landscape is characterized by several (almost) degenerate excitons [5, 56], the lowest excitons being at K and K' .

At zero temperature, only the degenerate excitons with momenta \mathbf{Q} at K and K' are populated. Along the path $\Gamma - K - \Gamma$, and for low values of n_c , the spectrum features a single sideband for momenta \mathbf{k} near K [Fig. 2(d)]. This is the replica of $\epsilon_{v\mathbf{k}-Q}$ with \mathbf{Q} at the inequivalent K point, which is the same as $\epsilon_{v\mathbf{k}}$ with \mathbf{k} around K' . The replica is shifted in energy by $\sim E_{\lambda Q}^{\text{eq}}$, and the intensity of the signal is proportional to $|A_{cv\mathbf{k}-Q}^{\lambda Q}|^2$, in agreement with Eq. (12). Increasing n_c , the exciton energies undergo a blue shift while the bandgap shrinks [Figs. 2(c) and (f)]. The replica of the valence band hybridizes with the conduction band, and the excitonic sideband acquires the shape of a mexican hat [well described by Eq. (17)], as shown in Fig. 2(g).

At temperatures $T = 70$ K, exciton states with momenta near other high symmetry points (M , Q and Γ) also become populated, see Fig. 2(b). Along the path $\Gamma - K - \Gamma$, and for low values of n_c , a second replica of the valence band appears for momenta \mathbf{k} near Q [Fig. 2(e)]. This emerges from excitons with $-\mathbf{Q}$ around Q , leading to a replica of $\epsilon_{v\mathbf{k}}$ with \mathbf{k} around K . As the exciton energies are almost degenerate, the two replicas in Fig. 2(e) are located in the same spectral range. Compared to Fig. 2(d), the signal appears blurred – this is due

to the presence of exciton states with momenta close to, but not exactly at, the high symmetry points. The additional excitonic sideband around the Q point persists at higher excitation densities, but its shape turns into a mexican hat, see Fig. 2(h), again in agreement with Eq. (17).

Conclusions.— We presented a first-principles approach to excitons in TR-ARPES, bridging the coherent and incoherent regimes through a unified formula that depends solely on the total number of excitons at the pump-probe delay τ . Applicable across a wide range of temperatures and excitation densities, our formula provides a powerful tool for understanding and engineering nonequilibrium band structures of excitonic materials. Band hybridization with dark excitons enables controlled shifts of the valence bands in both energy and momentum, and to reshape them into a mexican-hat dispersion. In particular, the mechanism of Ref. [38, 57] naturally extends to the incoherent regime, enabling control over the topological character of excited materials through exciton wavefunction symmetries. This points to a promising avenue for realizing nonequilibrium topological phases with lifetimes reaching the picosecond timescale.

ACKNOWLEDGMENTS

We acknowledge insightful discussions with Keshav Dani and Felipe da Jornada. We acknowledge funding from Ministero Università e Ricerca PRIN under grant agreement No. 2022WZ8LME, from INFN through project TIME2QUEST, from European Research Council MSCA-ITN TIMES under grant agreement 101118915, and from Tor Vergata University through project TESLA.

Appendix A: Finite excitation-density corrections

We here describe a practical method to estimate the finite-density corrections to the quasi-particle and exciton energies from the sole knowledge of the exciton populations $N_{\lambda Q}$.

Let $\rho_{\mu\mu'\mathbf{k}}(t) = -iG_{\mu\mu'\mathbf{k}}^<(t, t)$ be the one-electron density matrix at time t . We define $\rho_{\mu\mu'\mathbf{k}}^{\text{eq}} = \delta_{\mu\mu'} f_{\mu\mathbf{k}}^{\text{eq}}$ as the equilibrium one-electron density matrix, with equilibrium occupations $f_{v\mathbf{k}}^{\text{eq}} = 1$ and $f_{c\mathbf{k}}^{\text{eq}} = 0$. The change of the density matrix caused by an external pump pulse is then

$$\Delta\rho_{\mu\mu'\mathbf{k}}(t) = \rho_{\mu\mu'\mathbf{k}}(t) - \rho_{\mu\mu'\mathbf{k}}^{\text{eq}}. \quad (\text{A1})$$

This change induces the following change in the HSEX potential

$$V_{cc'\mathbf{k}}(t) = \sum_{vv'\mathbf{k}'} (v_{c\mathbf{k}v\mathbf{k}'v'\mathbf{k}'c'\mathbf{k}} - W_{c\mathbf{k}v\mathbf{k}'c'\mathbf{k}v'\mathbf{k}}) \Delta\rho_{v'v'\mathbf{k}'}(t) + \sum_{c_1c_2\mathbf{k}'} (v_{c\mathbf{k}c_1\mathbf{k}'c_2\mathbf{k}'c'\mathbf{k}} - W_{c\mathbf{k}c_1\mathbf{k}'c'\mathbf{k}c_2\mathbf{k}'}) \Delta\rho_{c_2c_1\mathbf{k}'}(t), \quad (\text{A2a})$$

$$V_{vv'\mathbf{k}}(t) = \sum_{cc'\mathbf{k}'} (v_{v\mathbf{k}c\mathbf{k}'c'\mathbf{k}'v'\mathbf{k}} - W_{v\mathbf{k}c\mathbf{k}'v'\mathbf{k}c'\mathbf{k}'}) \Delta\rho_{c'c'\mathbf{k}'}(t) + \sum_{v_1v_2\mathbf{k}'} (v_{v\mathbf{k}v_1\mathbf{k}'v_2\mathbf{k}'v'\mathbf{k}} - W_{v\mathbf{k}v_1\mathbf{k}'v'\mathbf{k}v_2\mathbf{k}'}) \Delta\rho_{v_2v_1\mathbf{k}'}(t), \quad (\text{A2b})$$

$$V_{cv\mathbf{k}}(t) = \sum_{v'c'\mathbf{k}'} (v_{c\mathbf{k}v'\mathbf{k}'c'\mathbf{k}'v\mathbf{k}} - W_{c\mathbf{k}v'\mathbf{k}'v\mathbf{k}c'\mathbf{k}'}) \Delta\rho_{c'v'\mathbf{k}'}(t) = - \sum_{v'c'\mathbf{k}'} K_{cv\mathbf{k},c'v'\mathbf{k}'}^0 \Delta\rho_{c'v'\mathbf{k}'}(t) = V_{cv\mathbf{k}}^*(t). \quad (\text{A2c})$$

In the HSEX approximation the renormalization of the quasiparticle energies can be estimated as

$$\epsilon_{\mu\mathbf{k}} = \epsilon_{\mu\mathbf{k}}^{\text{eq}} + V_{\mu\mu\mathbf{k}}, \quad (\text{A3})$$

where

$$V_{cck} \simeq \sum_{v'k'} (v_{ckv'k'v'k'ck} - W_{ckv'k'ckv'k'})(f_{v'k'} - 1) + \sum_{c'k'} (v_{ckc'k'c'k'ck} - W_{ckc'k'ckc'k'})f_{c'k'}, \quad (\text{A4a})$$

$$V_{vvk} \simeq \sum_{c'k'} (v_{vkc'k'c'k'vk} - W_{vkc'k'vkck})f_{c'k'} + \sum_{v'k'} (v_{vkv'k'v'k'vk} - W_{vkv'k'vkck})(f_{v'k'} - 1). \quad (\text{A4b})$$

In Eqs. (A4), the off-diagonal contributions of the density matrix are discarded, i.e., $\Delta\rho_{cc'k} \simeq \delta_{cc'}f_{ck}$ and $\Delta\rho_{vv'k} \simeq \delta_{vv'}(f_{vk} - 1)$. This is consistent with ignoring finite-density corrections to the quasiparticle wavefunctions. Thus, Eq. (A4) provides a formula for the renormalized quasi-particle energies in terms of the nonequilibrium occupations $f_{\mu k}$.

Let us now come to the renormalization of the exciton energies. At finite excitation density, the BSE for the exciton energies and wavefunctions reads

$$\sum_{c'v'k'} H_{cvk,c'v'k'}^Q \frac{A_{c'v'k'}^{\lambda Q}}{\sqrt{f_{v'k'} - f_{c'k'+Q}}} = E_{\lambda Q} \frac{A_{cvk}^{\lambda Q}}{\sqrt{f_{vk} - f_{ck+Q}}}, \quad (\text{A5})$$

with

$$H_{cvk,c'v'k'}^Q = \delta_{cvk,c'v'k'}(\epsilon_{ck+Q} - \epsilon_{vk}) - \sqrt{f_{vk} - f_{ck+Q}} K_{cvk,c'v'k'}^Q \sqrt{f_{v'k'} - f_{c'k'+Q}} \quad (\text{A6})$$

the BSE Hamiltonian. We rewrite Eq. (A6) as

$$H_{cvk,c'v'k'}^Q = H_{cvk,c'v'k'}^{\text{eq},Q} + \Delta H_{cvk,c'v'k'}^Q \quad (\text{A7})$$

where $H^{\text{eq},Q}$ is the equilibrium BSE Hamiltonian, calculated with equilibrium occupations $f_{vk}^{\text{eq}} = 1$ and $f_{ck}^{\text{eq}} = 0$, and equilibrium band structure $\epsilon_{\mu k} = \epsilon_{\mu k}^{\text{eq}}$. To lowest order in ΔH^Q we have

$$E_{\lambda Q} = E_{\lambda Q}^{\text{eq}} + \sum_{cvk} \sum_{c'v'k'} A_{cvk}^{\lambda Q*} \Delta H_{cvk,c'v'k'}^Q A_{c'v'k'}^{\lambda Q}, \quad (\text{A8})$$

where $E_{\lambda Q}^{\text{eq}}$ is the equilibrium exciton energy and $A_{cvk}^{\lambda Q}$ is the unperturbed exciton wavefunction.

We express ΔH^Q in terms of the nonequilibrium occupations $f_{\mu k}$. For the Pauli blocking factors we have

$$\sqrt{f_{vk} - f_{ck+Q}} \simeq 1 + \frac{1}{2}(f_{vk} - f_{ck+Q} - 1). \quad (\text{A9})$$

We conclude that to lowest order in the excitation density

$$\Delta H_{cvk,c'v'k'}^Q = \delta_{cvk,c'v'k'} \left[V_{cck+Q} - V_{vvk} \right] - \frac{1}{2}(f_{vk} - f_{ck+Q} + f_{vk'} - f_{ck'+Q} - 2) K_{cvk,c'v'k'}^Q, \quad (\text{A10})$$

where $V_{\mu\mu k}$ is given in Eq. (A4).

Equations (A3) and (A8) provide an approximation for the nonequilibrium quasi-particle energies and exciton energies in terms of the nonequilibrium occupations. To express these occupations in terms of exciton populations we observe that for small excitation densities the contribution of the λQ -exciton to f_{ck} is

$$\langle \lambda Q | \hat{d}_{ck}^\dagger \hat{d}_{ck} | \lambda Q \rangle = \sum_{c_1 v_1 k_1} \sum_{c_2 v_2 k_2} A_{c_1 v_1 k_1}^{\lambda Q*} A_{c_2 v_2 k_2}^{\lambda Q} \langle \Psi_g | \hat{d}_{v_1 k_1}^\dagger \hat{d}_{c_1 k_1 + Q} \hat{d}_{ck}^\dagger \hat{d}_{ck} \hat{d}_{c_2 k_2 + Q}^\dagger \hat{d}_{v_2 k_2} | \Psi_g \rangle = \sum_v |A_{cvk-Q}^{\lambda Q}|^2. \quad (\text{A11})$$

Therefore

$$f_{ck} = \sum_{\lambda Q v} N_{\lambda Q} |A_{cvk-Q}^{\lambda Q}|^2, \quad (\text{A12})$$

and similarly

$$f_{vk} = 1 - \sum_{\lambda Q c} N_{\lambda Q} |A_{cvk}^{\lambda Q}|^2. \quad (\text{A13})$$

Notice that the normalization of the exciton wavefunctions guarantees that $\sum_{ck} f_{ck} = \sum_{\lambda Q} N_{\lambda Q}$.

In Fig. 3 we compare the equilibrium band structure and exciton dispersions with those at moderate excitation density $n_c \simeq 10^{13} \text{ cm}^{-2}$ for the monolayer WSe₂. Due to finite density corrections the replica of high-energy valence bands intersect the low-energy conduction bands. In this scenario, the exciton-induced hybridization causes the typical mexican hat shape in TR-ARPES.

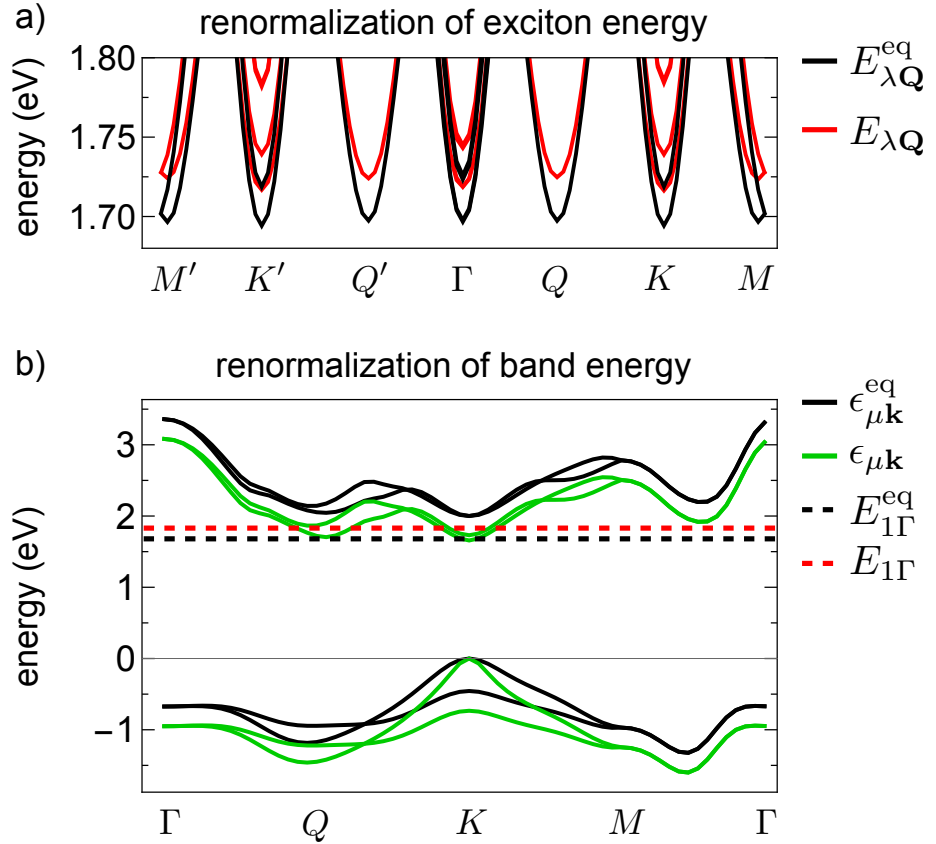


FIG. 3. Equilibrium and nonequilibrium [excitation density $n \simeq 10^{13} \text{ cm}^{-2}$] exciton dispersions (a) and quasiparticle energies (b). To highlight the band crossing between the conduction bands and the replica of the valence bands, dashed horizontal lines have been superimposed in correspondence of the energy of the lowest exciton with vanishing momentum.

Appendix B: Lehmann approach

The state of the system just *after* pumping ($t > 0$) can be written as

$$|\Psi(t)\rangle = |\Psi_g\rangle + \sum_{\lambda} \beta_{\lambda} e^{-iE_{\lambda 0}^{eq}t} |\lambda 0\rangle. \quad (\text{B1})$$

The coefficients β_{λ} are proportional to the excitonic polarizations since

$$\rho_{\lambda}(t) = \sum_{cv\mathbf{k}} A_{cv\mathbf{k}}^{\lambda 0*} \langle \Psi(t) | \hat{d}_{v\mathbf{k}}^{\dagger} \hat{d}_{c\mathbf{k}} | \Psi(t) \rangle = \sum_{cv\mathbf{k}} A_{cv\mathbf{k}}^{\lambda 0*} \sum_{\lambda'} \beta_{\lambda'} A_{cv\mathbf{k}}^{\lambda' 0} e^{-iE_{\lambda' 0}^{eq}t} = \beta_{\lambda} e^{-iE_{\lambda 0}^{eq}t}. \quad (\text{B2})$$

Thus, Eq. (B1) can also be written as

$$|\Psi(t)\rangle = |\Psi_g\rangle + \sum_{\lambda} \rho_{\lambda}(t) |\lambda 0\rangle. \quad (\text{B3})$$

For a pure state the Green's function is given by

$$G_{\mu\mu'\mathbf{k}}^<(t, t') \equiv i \langle \Psi(t') | \hat{d}_{\mu'\mathbf{k}}^{\dagger} e^{i\hat{H}(t-t')} \hat{d}_{\mu\mathbf{k}} | \Psi(t) \rangle, \quad (\text{B4})$$

where \hat{H} is the many-body Hamiltonian of the unperturbed system. We have

$$\hat{d}_{c'\mathbf{k}} |\Psi(t)\rangle = \sum_{\lambda} \beta_{\lambda} e^{-iE_{\lambda 0}^{eq}t} \sum_v A_{c'v\mathbf{k}}^{\lambda 0} \hat{d}_{v\mathbf{k}} |\Psi_g\rangle. \quad (\text{B5})$$

Taking into account that $\hat{H}\hat{d}_{v\mathbf{k}}|\Psi_g\rangle = -\epsilon_{v\mathbf{k}}^{\text{eq}}\hat{d}_{v\mathbf{k}}|\Psi_g\rangle$, we find for the Green's function in Eq. (B4)

$$G_{cc'\mathbf{k}}^<(t, t') = i \sum_{\lambda\lambda'v} \beta_\lambda^* \beta_{\lambda'} A_{c'v\mathbf{k}}^{\lambda\mathbf{0}*} A_{cv\mathbf{k}}^{\lambda'\mathbf{0}} e^{iE_{\lambda\mathbf{0}}^{\text{eq}}t'} e^{-iE_{\lambda'\mathbf{0}}^{\text{eq}}t} e^{-i\epsilon_{v\mathbf{k}}^{\text{eq}}(t-t')}. \quad (\text{B6})$$

This Green's function depends on t and t' separately, due to the interference of different exciton states [49, 58]. The Fourier transform with respect to $t - t'$ is dominated by the diagonal contributions and reads

$$G_{cc'\mathbf{k}}^<(\omega) = 2\pi i \sum_{\lambda v} |\rho_\lambda|^2 A_{c'v\mathbf{k}}^{\lambda\mathbf{0}*} A_{cv\mathbf{k}}^{\lambda\mathbf{0}} \delta(\omega - E_{\lambda\mathbf{0}}^{\text{eq}} - \epsilon_{v\mathbf{k}}^{\text{eq}}). \quad (\text{B7})$$

For low excitation densities, the coherence between $|\Psi_g\rangle$ and the exciton states $|\lambda\mathbf{0}\rangle$ is suppressed by electron-phonon scatterings on a timescale that varies from a few tens to a few hundreds of femtoseconds (depending on temperature and excitation densities) [33–35]. In the incoherent regime the polarization ρ_λ vanishes, and the electronic subsystem is described by an ensemble of bright and dark incoherent excitons. From the many-body density matrix of the ensemble $\hat{\rho} = |\Psi_g\rangle\langle\Psi_g| + \sum_{\lambda\mathbf{Q}} N_{\lambda\mathbf{Q}}^{\text{inc}} |\lambda\mathbf{Q}\rangle\langle\lambda\mathbf{Q}|$, with $N_{\lambda\mathbf{Q}}^{\text{inc}}$ the number of incoherent excitons, we can calculate the Green's function according to

$$G_{cc'\mathbf{k}}^<(t, t') = i\text{Tr}\left[\hat{\rho} e^{i\hat{H}t'} \hat{d}_{\mu'\mathbf{k}}^\dagger e^{i\hat{H}(t-t')} \hat{d}_{\mu\mathbf{k}} e^{-i\hat{H}t}\right] = \sum_{\lambda\mathbf{Q}} N_{\lambda\mathbf{Q}}^{\text{inc}} G_{cc'\mathbf{k}}^{\lambda\mathbf{Q}<}(t, t'), \quad (\text{B8})$$

where

$$\begin{aligned} G_{cc'\mathbf{k}}^{\lambda\mathbf{Q}<}(t, t') &= i\langle\lambda\mathbf{Q}(t')|\hat{d}_{c'\mathbf{k}}^\dagger e^{i\hat{H}(t-t')} \hat{d}_{c\mathbf{k}}|\lambda\mathbf{Q}(t)\rangle \\ &= ie^{-iE_{\lambda\mathbf{Q}}^{\text{eq}}(t-t')} \langle\lambda\mathbf{Q}|\hat{d}_{c'\mathbf{k}}^\dagger e^{i\hat{H}(t-t')} \hat{d}_{c\mathbf{k}}|\lambda\mathbf{Q}\rangle \\ &= ie^{-iE_{\lambda\mathbf{Q}}^{\text{eq}}(t-t')} \sum_v A_{c'v\mathbf{k}-\mathbf{Q}}^{\lambda\mathbf{Q}*} A_{cv\mathbf{k}-\mathbf{Q}}^{\lambda\mathbf{Q}} e^{-i\epsilon_{v\mathbf{k}-\mathbf{Q}}^{\text{eq}}(t-t')}. \end{aligned} \quad (\text{B9})$$

In the incoherent regime the Green's function depends exclusively on the time difference, and its Fourier transform reads

$$G_{cc'\mathbf{k}}^<(\omega) = 2\pi i \sum_{\lambda\mathbf{Q}v} N_{\lambda\mathbf{Q}}^{\text{inc}} A_{c'v\mathbf{k}-\mathbf{Q}}^{\lambda\mathbf{Q}*} A_{cv\mathbf{k}-\mathbf{Q}}^{\lambda\mathbf{Q}} \delta(\omega - E_{\lambda\mathbf{Q}}^{\text{eq}} - \epsilon_{v\mathbf{k}-\mathbf{Q}}^{\text{eq}}). \quad (\text{B10})$$

Notice that if the population of incoherent excitons is given by $N_{\lambda\mathbf{Q}}^{\text{inc}} = \delta_{\mathbf{Q},0}|\rho_\lambda|^2$, then the Green's function – and, consequently, the TR-ARPES spectrum – becomes identical for both the coherent and incoherent regimes. This can be verified by comparing Eq. (B10) with the expression for the Green's function in the coherent regime, i.e., Eq. (B7). Equations (B7) and (B10), derived from the Lehmann approach, agree with the Green's function in the many-body diagrammatic approximation HSEX+TX, see Eq. (12) in the main text.

Appendix C: HSEX self-energy for two bands

We consider a system with only one active conduction and valence bands. The HSEX lesser and greater Green's functions for resonant (not necessarily weak) pumping with the λ exciton have been derived in Ref. [36], and for sufficiently low temperatures they have a simple analytic form

$$G_{cc\mathbf{k}}^<(\omega) = 2\pi i \frac{E_{\lambda\mathbf{0}} + \epsilon_{v\mathbf{k}} - E_{\mathbf{k}}^-}{E_{\mathbf{k}}^+ - E_{\mathbf{k}}^-} \delta(\omega - E_{\mathbf{k}}^-), \quad (\text{C1a})$$

$$G_{cc\mathbf{k}}^>(\omega) = 2\pi i \frac{E_{\lambda\mathbf{0}} + \epsilon_{v\mathbf{k}} - E_{\mathbf{k}}^+}{E_{\mathbf{k}}^+ - E_{\mathbf{k}}^-} \delta(\omega - E_{\mathbf{k}}^+), \quad (\text{C1b})$$

where

$$E_{\mathbf{k}}^\pm \equiv \frac{1}{2} \left[\epsilon_{c\mathbf{k}} + E_{\lambda\mathbf{0}} + \epsilon_{v\mathbf{k}} \pm S_{\mathbf{k}} \right], \quad (\text{C2a})$$

$$S_{\mathbf{k}} \equiv \sqrt{(\epsilon_{c\mathbf{k}} - E_{\lambda\mathbf{0}} - \epsilon_{v\mathbf{k}})^2 + 4|\Delta_{\mathbf{k}}|^2}, \quad (\text{C2b})$$

$$\Delta_{\mathbf{k}} \equiv K_{cv\mathbf{k}}^{\lambda\mathbf{0}} \rho_\lambda. \quad (\text{C2c})$$

Setting $z = \omega + i\eta$, the retarded Green's function is then given by

$$G_{cc\mathbf{k}}^R(\omega) = i \int \frac{d\omega'}{2\pi} \frac{G_{cc\mathbf{k}}^>(\omega') - G_{cc\mathbf{k}}^<(\omega')}{z - \omega'} = \frac{z - E_{\lambda 0} - \epsilon_{v\mathbf{k}}}{(z - E_{\mathbf{k}}^+)(z - E_{\mathbf{k}}^-)} = \frac{1}{z - \epsilon_{c\mathbf{k}} - \frac{|\Delta_{\mathbf{k}}|^2}{z - E_{\lambda 0} - \epsilon_{v\mathbf{k}}}}, \quad (\text{C3})$$

from which we can read the retarded HSEX self-energy

$$\Sigma_{cc\mathbf{k}}^R(\omega) = \frac{|\Delta_{\mathbf{k}}|^2}{z - E_{\lambda 0} - \epsilon_{v\mathbf{k}}} - i\eta. \quad (\text{C4})$$

To obtain the lesser HSEX self-energy we observe that the Green's function in Eq. (C1a) can also be written as

$$G_{cc\mathbf{k}}^<(\omega) = G_{cc\mathbf{k}}^R(\omega) \Sigma_{cc\mathbf{k}}^<(\omega) G_{cc\mathbf{k}}^A(\omega). \quad (\text{C5})$$

Let us show that this relation is satisfied for

$$\Sigma_{cc\mathbf{k}}^<(\omega) = -f(\omega - E_{\lambda 0} - \epsilon_{v\mathbf{k}}) [\Sigma_{cc\mathbf{k}}^R(\omega) - \Sigma_{cc\mathbf{k}}^A(\omega)], \quad (\text{C6})$$

with $f(\omega) = 1/[e^{\omega/T} + 1]$ the Fermi function. We have

$$G_{cc\mathbf{k}}^R(\omega) [\Sigma_{cc\mathbf{k}}^R(\omega) - \Sigma_{cc\mathbf{k}}^A(\omega)] G_{cc\mathbf{k}}^A(\omega) = G_{cc\mathbf{k}}^R(\omega) - G_{cc\mathbf{k}}^A(\omega) = G_{cc\mathbf{k}}^>(\omega) - G_{cc\mathbf{k}}^<(\omega). \quad (\text{C7})$$

Therefore

$$G_{cc\mathbf{k}}^R(\omega) \Sigma_{cc\mathbf{k}}^<(\omega) G_{cc\mathbf{k}}^A(\omega) = -2\pi i f(\omega - E_{\lambda 0} - \epsilon_{v\mathbf{k}}) \left[\frac{E_{\lambda 0} + \epsilon_{v\mathbf{k}} - E_{\mathbf{k}}^+}{E_{\mathbf{k}}^+ - E_{\mathbf{k}}^-} \delta(\omega - E_{\mathbf{k}}^+) - \frac{E_{\lambda 0} + \epsilon_{v\mathbf{k}} - E_{\mathbf{k}}^-}{E_{\mathbf{k}}^+ - E_{\mathbf{k}}^-} \delta(\omega - E_{\mathbf{k}}^-) \right]. \quad (\text{C8})$$

Next we observe that Eq. (C2a) implies

$$\begin{aligned} E_{\mathbf{k}}^{\pm} - E_{\lambda 0} - \epsilon_{v\mathbf{k}} &= \frac{1}{2} \left[\epsilon_{c\mathbf{k}} + E_{\lambda 0} + \epsilon_{v\mathbf{k}} \pm S_{\mathbf{k}} \right] - E_{\lambda 0} - \epsilon_{v\mathbf{k}} \\ &= \frac{1}{2} \left[\epsilon_{c\mathbf{k}} - E_{\lambda 0} - \epsilon_{v\mathbf{k}} \pm \sqrt{(\epsilon_{c\mathbf{k}} - E_{\lambda 0} - \epsilon_{v\mathbf{k}})^2 + 4\Delta_{\mathbf{k}}^2} \right] \gtrless 0 \end{aligned} \quad (\text{C9})$$

We conclude the second term in Eq. (C8) dominates, and we recover the analytic result in Eq. (C1a).

Appendix D: HSEX self-energy for multiple bands

In the general case, the Green's function in the HSEX approximation can be obtained from the equation of motion on the Keldysh contour [46]

$$\left[i \frac{d}{dz} - \epsilon_{\mu\mathbf{k}}^{\text{eq}} \right] G_{\mu\mu'\mathbf{k}}(z, z') - \sum_{\nu} V_{\mu\nu\mathbf{k}}(t) G_{\nu\mu'\mathbf{k}}(z, z') = \delta(z, z'), \quad (\text{D1})$$

where the HSEX potential is given in Eqs. (A2). We look for an approximate solution of Eq. (D1) in the conduction subspace, which is the subspace we are interested in. We discard all matrix elements $V_{cc'}$ with $c \neq c'$ and $V_{vv'}$ with $v \neq v'$. This is equivalent to discard finite-density corrections to the quasiparticle wavefunctions. Although these corrections do not pose a conceptual problem, they considerably complicate the practical implementation of the theory. From Eq. (D1) we have

$$\left[i \frac{d}{dz} - \epsilon_{c\mathbf{k}} \right] G_{cc'\mathbf{k}}(z, z') - \sum_{\nu} V_{cv\mathbf{k}}(t) G_{\nu c'\mathbf{k}}(z, z') = \delta(z, z'), \quad (\text{D2a})$$

$$\left[i \frac{d}{dz} - \epsilon_{v\mathbf{k}} \right] G_{\nu c'\mathbf{k}}(z, z') - \sum_{c''} V_{\nu c''\mathbf{k}}(t) G_{c'' c'\mathbf{k}}(z, z') = 0, \quad (\text{D2b})$$

where $\epsilon_{\mu\mathbf{k}} \equiv \epsilon_{\mu\mathbf{k}}^{\text{eq}} + V_{\mu\mu\mathbf{k}}$ are the renormalized quasiparticle energies. The second equation is solved by

$$G_{\nu c'\mathbf{k}}(z, z') = \int d\bar{z} g_{v\mathbf{k}}(z, \bar{z}) \sum_{c''} V_{\nu c''\mathbf{k}}(\bar{t}) G_{c'' c'\mathbf{k}}(\bar{z}, z'), \quad (\text{D3})$$

where $g_{v\mathbf{k}}$ is the solution of

$$\left[i \frac{d}{dz} - \epsilon_{v\mathbf{k}} \right] g_{v\mathbf{k}}(z, z') = \delta(z, z'). \quad (\text{D4})$$

Inserting Eq. (D3) into Eq. (D2a) we find

$$\left[i \frac{d}{dz} - \epsilon_{c\mathbf{k}} \right] G_{cc'\mathbf{k}}(z, z') - \sum_{c''} \int d\bar{z} \Sigma_{cc''\mathbf{k}}(z, \bar{z}) G_{c''c'\mathbf{k}}(\bar{z}, z') = \delta(z, z'), \quad (\text{D5})$$

where the HSEX self-energy reads

$$\Sigma_{cc'\mathbf{k}}(z, z') = \sum_v V_{cv\mathbf{k}}(t) g_{v\mathbf{k}}(z, z') V_{c'v\mathbf{k}}^*(t'). \quad (\text{D6})$$

Equation (D6) can be further manipulated. The HSEX dynamics of the density matrix is governed by the equation of motion $i \frac{d}{dt} \rho_{\mathbf{k}} = [h_{\mathbf{k}}^{\text{HSEX}}, \rho_{\mathbf{k}}]$ with $h_{\mu\nu\mathbf{k}}^{\text{HSEX}} = \delta_{\mu\nu} \epsilon_{\mu\mathbf{k}}^{\text{eq}} + V_{\mu\nu\mathbf{k}}$. Therefore we have

$$\begin{aligned} i \frac{d}{dt} \rho_{cv\mathbf{k}} &= (\epsilon_{c\mathbf{k}}^{\text{eq}} - \epsilon_{v\mathbf{k}}^{\text{eq}}) \rho_{cv\mathbf{k}} + \sum_{c'} V_{cc'\mathbf{k}} \rho_{c'v\mathbf{k}} - \sum_{v'} \rho_{cv'\mathbf{k}} V_{v'v\mathbf{k}} + \sum_{v'} V_{cv'\mathbf{k}} \rho_{v'v\mathbf{k}} - \sum_{c'} \rho_{cc'\mathbf{k}} V_{c'v\mathbf{k}} \\ &\simeq (\epsilon_{c\mathbf{k}} - \epsilon_{v\mathbf{k}}) \rho_{cv\mathbf{k}} + (f_{v\mathbf{k}} - f_{c\mathbf{k}}) V_{cv\mathbf{k}}, \end{aligned} \quad (\text{D7})$$

where we implement the previously introduced approximations $V_{cc'\mathbf{k}} \simeq \delta_{cc'} V_{c\mathbf{k}c\mathbf{k}}$, $V_{vv'\mathbf{k}} \simeq \delta_{vv'} V_{v\mathbf{k}v\mathbf{k}}$, as well as $\rho_{cc'\mathbf{k}} \simeq \delta_{cc'} f_{c\mathbf{k}}$, $\rho_{vv'\mathbf{k}} \simeq \delta_{vv'} f_{v\mathbf{k}}$, $f_{\mu\mathbf{k}}$ being the occupation of the quasiparticle state $\mu\mathbf{k}$. Taking into account that the off-diagonal HSEX potential $V_{cv\mathbf{k}}(t)$ is given by Eq. (A2c), and comparing with the BSE in Eq. (A5), we see that Eq. (D7) is solved by

$$\rho_{cv\mathbf{k}}(t) = \sum_{\lambda} A_{cv\mathbf{k}}^{\lambda 0} \rho_{\lambda} e^{-iE_{\lambda 0} t}. \quad (\text{D8})$$

Ignoring the finite-density corrections to the exciton wavefunctions, we have

$$\sum_{c'v'\mathbf{k}'} K_{cv\mathbf{k}, c'v'\mathbf{k}'}^{\mathbf{0}} A_{c'v'\mathbf{k}'}^{\lambda 0} = (\epsilon_{c\mathbf{k}}^{\text{eq}} - \epsilon_{v\mathbf{k}}^{\text{eq}} - E_{\lambda 0}^{\text{eq}}) A_{cv\mathbf{k}}^{\lambda 0} = K_{cv\mathbf{k}}^{\lambda 0}, \quad (\text{D9})$$

and therefore $V_{cv\mathbf{k}}(t) = \sum_{\lambda} K_{cv\mathbf{k}}^{\lambda 0} \rho_{\lambda} e^{-iE_{\lambda 0} t}$. Substituting this result into Eq. (D6) we obtain

$$\Sigma_{cc'\mathbf{k}}(z, z') = \sum_{v\lambda\lambda'} K_{cv\mathbf{k}}^{\lambda 0} \rho_{\lambda} e^{-iE_{\lambda 0} t} g_{v\mathbf{k}}(z, z') e^{iE_{\lambda' 0} t'} K_{c'v\mathbf{k}}^{\lambda' 0*} \rho_{\lambda'}^*. \quad (\text{D10})$$

Let us extract the retarded component of the self-energy. From Eq. (D4) we have

$$g_{v\mathbf{k}}^R(t, t') = -i\theta(t - t') e^{-i\epsilon_{v\mathbf{k}}(t-t')}. \quad (\text{D11})$$

For sufficiently long probes, beating terms can be ignored [49, 58]. Retaining only terms with $\lambda = \lambda'$, the retarded component of Eq. (D10) in frequency space reads

$$\Sigma_{cc'\mathbf{k}}^R(\omega) = \sum_{\lambda v} K_{cv\mathbf{k}}^{\lambda 0} \frac{|\rho_{\lambda}|^2}{z - E_{\lambda 0} - \epsilon_{v\mathbf{k}}} K_{c'v\mathbf{k}}^{\lambda 0*} - i\eta. \quad (\text{D12})$$

This formula generalizes Eq. (C4) to multiple bands. Accordingly, the generalization of Eq. (C6) for the lesser self-energy is

$$\Sigma_{cc'\mathbf{k}}^<(\omega) = - \sum_{\lambda v} f(\omega - E_{\lambda 0} - \epsilon_{v\mathbf{k}}) \left[K_{cv\mathbf{k}}^{\lambda 0} \left(\frac{|\rho_{\lambda}|^2}{z - E_{\lambda 0} - \epsilon_{v\mathbf{k}}} - \frac{|\rho_{\lambda}|^2}{z^* - E_{\lambda 0} - \epsilon_{v\mathbf{k}}} \right) K_{c'v\mathbf{k}}^{\lambda 0*} - 2i\eta \right]. \quad (\text{D13})$$

Equations (D12) and (D13) are the self-energies of the main text for the coherent regime, i.e., Eqs. (4) with σ evaluated in $N_{\lambda\mathbf{Q}} = \delta_{\mathbf{Q}0} |\rho_{\lambda}|^2$.

Appendix E: TX self-energy

We expand the xc function in the excitonic basis [32, 41]

$$L_{c_1 v_1 \mathbf{k}_1, c_2 v_2 \mathbf{k}_2}^{\lambda \mathbf{Q}}(t, t') = \sum_{\lambda} A_{c_1 v_1 \mathbf{k}_1}^{\lambda \mathbf{Q}} N_{\lambda \mathbf{Q}}^{\leq} e^{-iE_{\lambda \mathbf{Q}}(t-t')} A_{c_2 v_2 \mathbf{k}_2}^{\lambda \mathbf{Q}^*}, \quad (\text{E1})$$

with $N_{\lambda \mathbf{Q}}^{\leq} = N_{\lambda \mathbf{Q}}^{\text{inc}}$ and $N_{\lambda \mathbf{Q}}^{\geq} = 1 + N_{\lambda \mathbf{Q}}^{\text{inc}}$, and approximate the Green's function at the quasiparticle level, $G_{v \mathbf{k}}^{\leq}(t, t') = i f_{v \mathbf{k}}^{\leq} e^{-i\epsilon_{v \mathbf{k}}(t-t')}$, with $f_{v \mathbf{k}}^{\leq} = f_{v \mathbf{k}}$ and $f_{v \mathbf{k}}^{\geq} = f_{v \mathbf{k}} - 1$. Then, the Fourier transform of the lesser and greater TX self-energy, see Eq. (10), read

$$\Sigma_{cc' \mathbf{k}}^{\leq}(\omega) = 2\pi i \sum_{\lambda \mathbf{Q} v} K_{cv \mathbf{k}}^{\lambda \mathbf{Q}} N_{\lambda \mathbf{Q}}^{\leq} f_{v \mathbf{k} - \mathbf{Q}}^{\leq} K_{c' v \mathbf{k}}^{\lambda \mathbf{Q}^*} \delta(\omega - E_{\lambda \mathbf{Q}} - \epsilon_{v \mathbf{k} - \mathbf{Q}}). \quad (\text{E2})$$

The retarded TX self-energy can be calculated from

$$\Sigma_{cc' \mathbf{k}}^R(\omega) = i \int \frac{d\omega'}{2\pi} \frac{\Sigma_{cc' \mathbf{k}}^>(\omega) - \Sigma_{cc' \mathbf{k}}^<(\omega)}{\omega - \omega' + i\eta} - i\eta = \sum_{\lambda \mathbf{Q} v} K_{cv \mathbf{k}}^{\lambda \mathbf{Q}} \frac{N_{\lambda \mathbf{Q}} + 1 - f_{v \mathbf{k} - \mathbf{Q}}}{\omega - E_{\lambda \mathbf{Q}} - \epsilon_{v \mathbf{k} - \mathbf{Q}} + i\eta} K_{c' v \mathbf{k}}^{\lambda \mathbf{Q}^*} - i\eta. \quad (\text{E3})$$

For not too large excitation densities, we can approximate $1 - f_{v \mathbf{k} - \mathbf{Q}} \simeq 0$, thus recovering the result in the main text. In analogy with Eq. (D13), we approximate the lesser TX self-energy as

$$\Sigma_{cc' \mathbf{k}}^<(\omega) = - \sum_{\lambda \mathbf{Q} v} f(\omega - E_{\lambda \mathbf{Q}} - \epsilon_{v \mathbf{k} - \mathbf{Q}}) \left[K_{cv \mathbf{k}}^{\lambda \mathbf{Q}} \left(\frac{N_{\lambda \mathbf{Q}}}{z - E_{\lambda \mathbf{Q}} - \epsilon_{v \mathbf{k} - \mathbf{Q}}} - \frac{N_{\lambda \mathbf{Q}}}{z^* - E_{\lambda \mathbf{Q}} - \epsilon_{v \mathbf{k} - \mathbf{Q}}} \right) K_{c' v \mathbf{k}}^{\lambda \mathbf{Q}^*} - 2i\eta \right]. \quad (\text{E4})$$

Equations (E3) and (E4) are the self-energies of the main text for the incoherent regime, i.e., Eqs. (4) with σ evaluated in $N_{\lambda \mathbf{Q}} = N_{\lambda \mathbf{Q}}^{\text{inc}}$.

Appendix F: Numerical details

The electronic structure is described using a spin-resolved density functional theory (DFT) band dispersion $\epsilon_{n \mathbf{k}}$, mapped onto a tight-binding representation as detailed in Ref. [59]. To match the experimentally measured quasiparticle band gap of about 2.0 eV, a rigid scissor correction of 0.5 eV is applied to the conduction-band states $\epsilon_{c \mathbf{k}}$ [60, 61]. The eigenstates of the Bloch Hamiltonian, denoted by $\mathbf{U}_{\mathbf{k}}$, serve as the basis for constructing the Coulomb matrix elements that appear in both the Bethe–Salpeter equation (BSE) kernel and the Hartree–screened-exchange (HSEX) Hamiltonian, following the methodology of Ref. [28].

The Coulomb interaction is modeled using the Rytova–Keldysh potential [62, 63], assuming a dielectric constant $\epsilon = 1$ and a screening length of $r_0 = 45 \text{ \AA}$ [64]. To treat the divergence of the Coulomb potential $v_{\mathbf{q}}$ near the Γ point, we adopt the regularization scheme introduced in Refs. [65, 66], which consists of averaging $v_{\mathbf{q}}$ over a small region Ω around $\mathbf{q} = 0$. The size of this region is determined by the spacing of the Brillouin-zone sampling grid.

In typical semiconductors, Coulomb matrix elements that involve processes changing the number of electrons in the valence or conduction bands are vanishingly small and are therefore neglected [67]. Since the Rytova–Keldysh interaction tensor V in Eq. (5) already incorporates *ab initio* static screening over the momentum scales relevant for excitonic physics, the screened exchange interaction W entering both the BSE kernel and the HSEX Hamiltonian is approximated by $W \approx V$. This simplification has been demonstrated to reproduce experimental exciton binding energies with high accuracy in two-dimensional systems [60, 68, 69].

In the calculations presented here, the electronic subspace is limited to the two uppermost valence bands and the two lowest conduction bands. The Brillouin zone is sampled using a uniform mesh comprising 3072 \mathbf{k} points.

[1] G. Onida, L. Reining, and A. Rubio, Electronic excitations: density-functional versus many-body green's-function approaches, *Rev. Mod. Phys.* **74**, 601 (2002).
[2] H. Zhang, T. Pincelli, C. Jozwiak, T. Kondo, R. Ernstor-

fer, T. Sato, and S. Zhou, Angle-resolved photoemission spectroscopy, *Nature Reviews Methods Primers* **2**, 54 (2022).

[3] F. Boschini, M. Zonno, and A. Damascelli, Time-resolved arpes studies of quantum materials, *Rev. Mod. Phys.* **96**, 015003 (2024).

[4] C. Xu and A. Zong, Time-domain study of coupled collective excitations in quantum materials, *npj Quantum Materials* **10**, 21 (2025).

[5] J. Madéo, M. K. L. Man, C. Sahoo, M. Campbell, V. Parrekk, E. L. Wong, A. Al-Mahboob, N. S. Chan, A. Karmakar, B. M. K. Mariserla, X. Li, T. F. Heinz, T. Cao, and K. M. Dani, Directly visualizing the momentum-forbidden dark excitons and their dynamics in atomically thin semiconductors, *Science* **370**, 1199 (2020).

[6] M. Dendzik, R. P. Xian, E. Perfetto, D. Sangalli, D. Kutyakov, S. Dong, S. Beaulieu, T. Pincelli, F. Pressacco, D. Curcio, S. Y. Agustsson, M. Heber, J. Hauer, W. Wurth, G. Brenner, Y. Acremann, P. Hofmann, M. Wolf, A. Marini, G. Stefanucci, L. Rettig, and R. Ernstorfer, Observation of an excitonic mott transition through ultrafast core-cum-conduction photoemission spectroscopy, *Phys. Rev. Lett.* **125**, 096401 (2020).

[7] H. Tanimura and K. Tanimura, Time- and angle-resolved photoemission spectroscopy for the saddle-point excitons in GaAs, *Phys. Rev. B* **102**, 045204 (2020).

[8] R. Wallauer, R. Perea-Causin, L. Münster, S. Zajusch, S. Brem, J. Gütde, K. Tanimura, K.-Q. Lin, R. Huber, E. Malic, and U. Höfer, Momentum-resolved observation of exciton formation dynamics in monolayer WS₂, *Nano Letters* **21**, 5867 (2021).

[9] K. Fukutani, R. Stania, C. Il Kwon, J. S. Kim, K. J. Kong, J. Kim, and H. W. Yeom, Detecting photoelectrons from spontaneously formed excitons, *Nature Physics* **17**, 1024 (2021).

[10] A. Kunin, S. Chernov, J. Bakalis, Z. Li, S. Cheng, Z. H. Withers, M. G. White, G. Schönhense, X. Du, R. K. Kawakami, and T. K. Allison, Momentum-resolved exciton coupling and valley polarization dynamics in monolayer ws₂, *Phys. Rev. Lett.* **130**, 046202 (2023).

[11] J. P. Bange, D. Schmitt, W. Bennecke, G. Meneghini, A. AlMutairi, K. Watanabe, T. Taniguchi, D. Steil, S. Steil, R. T. Weitz, G. S. M. Jansen, S. Hofmann, S. Brem, E. Malic, M. Reutzel, and S. Mathias, Probing electron-hole coulomb correlations in the exciton landscape of a twisted semiconductor heterostructure, *Science Advances* **10**, eadi1323 (2024).

[12] V. Gosetti, J. Cervantes-Villanueva, S. Mor, D. Sangalli, A. García-Cristóbal, A. Molina-Sánchez, V. F. Agekyan, M. Tuniz, D. Puntel, W. Bronsch, F. Cilento, and S. Pagliara, *Unveiling exciton formation: exploring the early stages in time, energy and momentum domain* (2024), arXiv:2412.02507 [cond-mat.mtrl-sci].

[13] M. K. L. Man, J. Madéo, C. Sahoo, K. Xie, M. Campbell, V. Parrekk, A. Karmakar, E. L. Wong, A. Al-Mahboob, N. S. Chan, D. R. Bacon, X. Zhu, M. M. M. Abdelrasoul, X. Li, T. F. Heinz, F. H. da Jornada, T. Cao, and K. M. Dani, Experimental measurement of the intrinsic excitonic wave function, *Science Advances* **7**, eabg0192 (2021).

[14] S. Dong, M. Puppin, T. Pincelli, S. Beaulieu, D. Christiansen, H. Hübener, C. W. Nicholson, R. P. Xian, M. Dendzik, Y. Deng, Y. W. Windsor, M. Selig, E. Malic, A. Rubio, A. Knorr, M. Wolf, L. Rettig, and R. Ernstorfer, Direct measurement of key exciton properties: Energy, dynamics, and spatial distribution of the wave function, *Natural Sciences* **1**, e10010 (2021).

[15] G. Meneghini, M. Reutzel, S. Mathias, S. Brem, and E. Malic, Hybrid exciton signatures in arpes spectra of van der waals materials, *ACS Photonics* **10**, 3570 (2023).

[16] R. Mori, S. Ciocys, K. Takasan, P. Ai, K. Currier, T. Morimoto, J. E. Moore, and A. Lanzara, Spin-polarized spatially indirect excitons in a topological insulator, *Nature* **614**, 249 (2023).

[17] M. Na, A. K. Mills, and D. J. Jones, Advancing time- and angle-resolved photoemission spectroscopy: The role of ultrafast laser development, *Physics Reports* **1036**, 1 (2023).

[18] H. Haug and S. W. Koch, *Quantum theory of the optical and electronic properties of semiconductors* (world scientific, 2009).

[19] M. Lindberg and S. W. Koch, Effective bloch equations for semiconductors, *Phys. Rev. B* **38**, 3342 (1988).

[20] T. Östreich and K. Schönhammer, Non-stationary excitonic-insulator states in photoexcited semiconductors, *Zeitschrift für Physik B Condensed Matter* **91**, 189 (1993).

[21] K. Hannewald, S. Glutsch, and F. Bechstedt, Excitonic insulator through coherent pulse excitation?, *Journal of Physics: Condensed Matter* **13**, 275 (2000).

[22] S. W. Koch, M. Kira, G. Khitrova, and H. M. Gibbs, Semiconductor excitons in new light, *Nature Materials* **5**, 523 (2006).

[23] A. B. Madrid, K. Hyeon-Deuk, B. F. Habenicht, and O. V. Prezhdo, Phonon-induced dephasing of excitons in semiconductor quantum dots: Multiple exciton generation, fission, and luminescence, *ACS Nano* **3**, 2487 (2009).

[24] Z. Nie, R. Long, L. Sun, C.-C. Huang, J. Zhang, Q. Xiong, D. W. Hewak, Z. Shen, O. V. Prezhdo, and Z.-H. Loh, Ultrafast carrier thermalization and cooling dynamics in few-layer MoS₂, *ACS Nano* **8**, 10931 (2014).

[25] P. Dey, J. Paul, Z. Wang, C. E. Stevens, C. Liu, A. H. Romero, J. Shan, D. J. Hilton, and D. Karaiskaj, Optical coherence in atomic-monolayer transition-metal dichalcogenides limited by electron-phonon interactions, *Phys. Rev. Lett.* **116**, 127402 (2016).

[26] D. Sangalli, E. Perfetto, G. Stefanucci, and A. Marini, An ab-initio approach to describe coherent and non-coherent exciton dynamics, *The European Physical Journal B* **91**, 171 (2018).

[27] G. Stefanucci and E. Perfetto, From carriers and virtual excitons to exciton populations: Insights into time-resolved arpes spectra from an exactly solvable model, *Phys. Rev. B* **103**, 245103 (2021).

[28] E. Perfetto and G. Stefanucci, Real-time GW-Ehrenfest-Fan-Migdal method for nonequilibrium 2d materials, *Nano Letters* **23**, 7029 (2023).

[29] R. Bertoni, C. W. Nicholson, L. Waldecker, H. Hübener, C. Monney, U. De Giovannini, M. Puppin, M. Hoesch, E. Springate, R. T. Chapman, C. Cacho, M. Wolf, A. Rubio, and R. Ernstorfer, Generation and evolution of spin-, valley-, and layer-polarized excited carriers in inversion-symmetric WSe₂, *Phys. Rev. Lett.* **117**, 277201 (2016).

[30] S. Z. Uddin, H. Kim, M. Lorenzon, M. Yeh, D.-H. Lien, E. S. Barnard, H. Htoon, A. Weber-Bargioni, and A. Javey, Neutral exciton diffusion in monolayer MoS₂, *ACS Nano* **14**, 13433 (2020).

[31] E. Perfetto and G. Stefanucci, Ultrafast creation and melting of nonequilibrium excitonic condensates in bulk WSe₂, *Phys. Rev. B* **103**, L241404 (2021).

[32] G. Stefanucci and E. Perfetto, Excitonic Bloch equations from first principles, *SciPost Phys.* **18**, 009 (2025).

[33] G. Moody, C. Kavir Dass, K. Hao, C.-H. Chen, L.-J. Li, A. Singh, K. Tran, G. Clark, X. Xu, G. Berghäuser, E. Malic, A. Knorr, and X. Li, Intrinsic homogeneous linewidth and broadening mechanisms of excitons in monolayer transition metal dichalcogenides, *Nature Communications* **6**, 8315 (2015).

[34] M. Selig, G. Berghäuser, A. Raja, P. Nagler, C. Schüller, T. F. Heinz, T. Korn, A. Chernikov, E. Malic, and A. Knorr, Excitonic linewidth and coherence lifetime in monolayer transition metal dichalcogenides, *Nature Communications* **7**, 13279 (2016).

[35] T. Jakubczyk, K. Nogajewski, M. R. Molas, M. Bartos, W. Langbein, M. Potemski, and J. Kasprzak, Impact of environment on dynamics of exciton complexes in a ws₂ monolayer, *2D Materials* **5**, 031007 (2018).

[36] E. Perfetto, D. Sangalli, A. Marini, and G. Stefanucci, Pump-driven normal-to-excitonic insulator transition: Josephson oscillations and signatures of BEC-BCS crossover in time-resolved ARPES, *Phys. Rev. Materials* **3**, 124601 (2019).

[37] E. Perfetto, S. Bianchi, and G. Stefanucci, Time-resolved arpes spectra of nonequilibrium excitonic insulators: Revealing macroscopic coherence with ultrashort pulses, *Phys. Rev. B* **101**, 041201 (2020).

[38] E. Perfetto and G. Stefanucci, Floquet topological phase of non-driven *p*-wave nonequilibrium excitonic insulators, *Phys. Rev. Lett.* **125**, 106401 (2020).

[39] Y.-H. Chan, D. Y. Qiu, F. H. da Jornada, and S. G. Louie, Giant self-driven exciton-floquet signatures in time-resolved photoemission spectroscopy of MoS₂ from time-dependent GW approach, *Proceedings of the National Academy of Sciences* **120**, e2301957120 (2023).

[40] V. Pareek, D. R. Bacon, X. Zhu, Y.-H. Chan, F. Bussolotti, M. G. Menezes, N. S. Chan, J. P. Urquiza, K. Watanabe, T. Taniguchi, E. Perfetto, M. K. L. Man, J. Madéo, G. Stefanucci, D. Y. Qiu, K. E. J. Goh, F. H. da Jornada, and K. M. Dani, Driving floquet physics with excitonic fields, *Nature Physics* **10.1038/s41567-025-03132-z** (2026).

[41] E. Perfetto, D. Sangalli, A. Marini, and G. Stefanucci, First-principles approach to excitons in time-resolved and angle-resolved photoemission spectra, *Phys. Rev. B* **94**, 245303 (2016).

[42] A. Steinhoff, M. Florian, M. Rösner, G. Schönhoff, T. O. Wehling, and F. Jahnke, Exciton fission in monolayer transition metal dichalcogenide semiconductors, *Nature Communications* **8**, 1166 (2017).

[43] A. Rustagi and A. F. Kemper, Photoemission signature of excitons, *Phys. Rev. B* **97**, 235310 (2018).

[44] D. Christiansen, M. Selig, E. Malic, R. Ernstorfer, and A. Knorr, Theory of exciton dynamics in time-resolved arpes: Intra- and intervalley scattering in two-dimensional semiconductors, *Phys. Rev. B* **100**, 205401 (2019).

[45] J. K. Freericks, H. R. Krishnamurthy, and T. Pruschke, Theoretical description of time-resolved photoemission spectroscopy: Application to pump-probe experiments, *Phys. Rev. Lett.* **102**, 136401 (2009).

[46] G. Stefanucci and R. van Leeuwen, *Nonequilibrium Many-Body Theory of Quantum Systems: A Modern Introduction*, 2nd ed. (Cambridge University Press, 2025).

[47] A. Thränhardt, S. Kuckenburg, A. Knorr, T. Meier, and S. W. Koch, Quantum theory of phonon-assisted exciton formation and luminescence in semiconductor quantum wells, *Phys. Rev. B* **62**, 2706 (2000).

[48] S. Brem, M. Selig, G. Berghaeuser, and E. Malic, Exciton relaxation cascade in two-dimensional transition metal dichalcogenides, *Scientific Reports* **8**, 8238 (2018).

[49] Z. Zhang, W. Hu, E. Perfetto, and G. Stefanucci, Long-lived coherence between incoherent excitons revealed by time-resolved angle-resolved photoemission spectroscopy: An exact solution, *Phys. Rev. B* **111**, 235124 (2025).

[50] H.-Y. Chen, D. Sangalli, and M. Bernardi, First-principles ultrafast exciton dynamics and time-domain spectroscopies: Dark-exciton mediated valley depolarization in monolayer WSe₂, *Phys. Rev. Res.* **4**, 043203 (2022).

[51] D. Kremp, W. Kraeft, and A. Lambert, Equation of state and ionization equilibrium for nonideal plasmas, *Physica A: Statistical Mechanics and its Applications* **127**, 72 (1984).

[52] D. Semkat, F. Richter, D. Kremp, G. Manzke, W.-D. Kraeft, and K. Henneberger, Ionization equilibrium in an excited semiconductor: Mott transition versus bose-einstein condensation, *Phys. Rev. B* **80**, 155201 (2009).

[53] G. Strinati, Application of the green's functions method to the study of the optical properties of semiconductors, *La Rivista del Nuovo Cimento (1978-1999)* **11**, 1 (1988).

[54] A tiny difference may arise from the polaronic-like shift of the exciton energy in the incoherent regime, see Ref. [27].

[55] K.-Q. Lin, C. S. Ong, S. Bange, P. E. Faria Junior, B. Peng, J. D. Ziegler, J. Zipfel, C. Bäuml, N. Paradiso, K. Watanabe, T. Taniguchi, C. Strunk, B. Monserrat, J. Fabian, A. Chernikov, D. Y. Qiu, S. G. Louie, and J. M. Lupton, Narrow-band high-lying excitons with negative-mass electrons in monolayer wse₂, *Nature Communications* **12**, 5500 (2021).

[56] T. Deilmann and K. S. Thygesen, Finite-momentum exciton landscape in mono- and bilayer transition metal dichalcogenides, *2D Materials* **6**, 035003 (2019).

[57] M. S. Foster, V. Gurarie, M. Dzero, and E. A. Yuzbashyan, Quench-induced floquet topological *p*-wave superfluids, *Phys. Rev. Lett.* **113**, 076403 (2014).

[58] A. Rustagi and A. F. Kemper, Coherent excitonic quantum beats in time-resolved photoemission measurements, *Phys. Rev. B* **99**, 125303 (2019).

[59] G.-B. Liu, W.-Y. Shan, Y. Yao, W. Yao, and D. Xiao, Three-band tight-binding model for monolayers of group-vib transition metal dichalcogenides, *Phys. Rev. B* **88**, 085433 (2013).

[60] A. Chernikov, T. C. Berkelbach, H. M. Hill, A. Rigosi, Y. Li, B. Aslan, D. R. Reichman, M. S. Hybertsen, and T. F. Heinz, Exciton binding energy and nonhydrogenic rydberg series in monolayer ws₂, *Phys. Rev. Lett.* **113**, 076802 (2014).

[61] W.-T. Hsu, J. Quan, C.-Y. Wang, L.-S. Lu, M. Campbell, W.-H. Chang, L.-J. Li, X. Li, and C.-K. Shih, Dielectric impact on exciton binding energy and quasiparticle bandgap in monolayer ws₂ and wse₂, *2D Materials* **6**, 025028 (2019).

[62] L. V. Keldysh, Coulomb interaction in thin semiconductor and semimetal films, *Soviet Journal of Experimental and Theoretical Physics Letters* **29**, 658 (1979).

[63] P. Cudazzo, I. V. Tokatly, and A. Rubio, Dielectric screening in two-dimensional insulators: Implications for excitonic and impurity states in graphane, *Phys. Rev. B* **84**, 085406 (2011).

[64] A. V. Stier, N. P. Wilson, K. A. Velizhanin, J. Kono, X. Xu, and S. A. Crooker, Magnetooptics of exciton rydberg states in a monolayer semiconductor, *Phys. Rev. Lett.* **120**, 057405 (2018).

[65] F. Hüser, T. Olsen, and K. S. Thygesen, How dielectric screening in two-dimensional crystals affects the convergence of excited-state calculations: Monolayer mos₂, *Phys. Rev. B* **88**, 245309 (2013).

[66] E. Ridolfi, C. H. Lewenkopf, and V. M. Pereira, Excitonic structure of the optical conductivity in mos₂ monolayers, *Phys. Rev. B* **97**, 205409 (2018).

[67] R. E. Groenewald, M. Rösner, G. Schönhoff, S. Haas, and T. O. Wehling, Valley plasmonics in transition metal dichalcogenides, *Phys. Rev. B* **93**, 205145 (2016).

[68] A. Steinhoff, M. Rösner, F. Jahnke, T. O. Wehling, and C. Gies, Influence of excited carriers on the optical and electronic properties of mos₂, *Nano Letters* **14**, 3743 (2014).

[69] T. C. Berkelbach, M. S. Hybertsen, and D. R. Reichman, The-

ory of neutral and charged excitons in monolayer transition

metal dichalcogenides, *Phys. Rev. B* **88**, 045318 (2013).